


## RESEARCH ARTICLE OPEN ACCESS

# Design, Synthesis and Anti-Influenza Virus Activity of 4-*Tert*-Butyl-*N*-(3-Oxo-1-Thia-4-Azaspiro[4.5]Dec-4-yl) Benzamide Derivatives That Target Hemagglutinin-Mediated Fusion

Gözde Çınar<sup>1,2</sup>  | Zeynep Alikadioğlu<sup>3</sup> | Özge Soylu-Eter<sup>4</sup> | Lieve Naesens<sup>5</sup> | Gökçe Cihan-Üstündağ<sup>3</sup>

<sup>1</sup>Institute of Health Sciences, Istanbul University, Istanbul, Turkey | <sup>2</sup>Department of Pharmaceutical Chemistry, Faculty of Pharmacy, Istanbul Health and Technology University, Istanbul, Turkey | <sup>3</sup>Department of Pharmaceutical Chemistry, Faculty of Pharmacy, Istanbul University, Istanbul, Turkey | <sup>4</sup>Department of Pharmaceutical Technology, Faculty of Pharmacy, Firat University, Elazığ, Turkey | <sup>5</sup>Department of Microbiology, Immunology and Transplantation, Rega Institute for Medical Research, KU Leuven, Leuven, Belgium

**Correspondence:** Gözde Çınar ([gozde.cinar@istun.edu.tr](mailto:gozde.cinar@istun.edu.tr))

**Received:** 8 November 2024 | **Revised:** 28 February 2025 | **Accepted:** 8 March 2025

**Funding:** We would like to thank Professor Gültaze Çapan for sharing expertise in medicinal chemistry. L.N. wishes to thank the team of L. Persoons for dedicated technical assistance. This workstudy was supported by Scientific Research Projects Coordination Unit of Istanbul University (Grant Number: 32246).

**Keywords:** antiviral | hemagglutinin | influenza virus | spirothiazolidinone | synthesis

## ABSTRACT

Hemagglutinin (HA) is a viral glycoprotein that mediates influenza virus entry into the host cell and is considered a relevant viral target. We here report the identification of a class of 4-*tert*-butylphenyl-substituted spirothiazolidinones as HA-mediated fusion inhibitors with specific activity against influenza A/H3N2 virus. The novel spirocyclic compounds were achieved by using one-pot cyclocondensation method and the chemical structures were characterized by IR, <sup>1</sup>H NMR, <sup>13</sup>C NMR, and elemental analysis. Compound **2c**, bearing methyl substitutions at positions 2- and 8- of the spiro ring displayed an EC<sub>50</sub> value against influenza A/H3N2 virus of 1.3 μM and an antiviral selectivity index of 30. The fusion-inhibiting effect of compound **2c** was revealed in the polykaryon assay which is based on cell-cell fusion when influenza virus H3 HA-transfected cells are exposed to low pH. Computer-aided docking was performed to predict the possible binding pocket in the H3 HA trimer. Resistance data and *in silico* studies indicated that compound **2c** has an overlapping binding pocket in the stem region of H3 HA with the known fusion inhibitors TBHQ and arbidol.

## 1 | Introduction

Influenza viruses are negative sense, single-stranded RNA viruses that belong to the Orthomyxoviridae family. Three types of influenza virus (A, B, and C) cause disease in humans. While influenza A virus (IAV) and influenza B virus (IBV) undergo continuous antigenic drift to cause annual epidemics, the sporadic flu pandemics are due to emergence of antigenically novel IAV strains (Monto and Fukuda 2019). Since the turn of the

twentieth century, we have witnessed five IAV pandemics: in 1918 (Spanish influenza, H1N1), 1957 (Asian influenza, H2N2), 1968 (Hong Kong influenza, H3N2), 1977 (H1N1) and 2009 (H1N1). Besides, avian H5N1 or H7N9 IAVs occasionally infect humans to cause severe respiratory disease with high case-fatality rate (Harrington et al. 2021; Neumann and Kawaoka 2019). Also, the recent outbreak of an avian H5N1 IAV in dairy cattle requires vigilant monitoring (Neumann and Kawaoka 2024).

This is an open access article under the terms of the [Creative Commons Attribution-NonCommercial-NoDerivs](https://creativecommons.org/licenses/by-nc-nd/4.0/) License, which permits use and distribution in any medium, provided the original work is properly cited, the use is non-commercial and no modifications or adaptations are made.

© 2025 The Author(s). *Drug Development Research* published by Wiley Periodicals LLC.

The envelope of IAV particles carries three viral proteins, i.e. hemagglutinin (HA), neuraminidase (NA), and the M2 proton channel. The latter two are targeted by two classes of antiviral drugs that have been available since many years. The M2 channel blockers, amantadine and rimantadine, are restricted to IAV (Uyeki et al. 2022) and exhibit neurological side-effects. They are currently no longer recommended due to widespread resistance among circulating IAV strains (Dong et al. 2015; Batool et al. 2023). The NA inhibitors, oseltamivir, zanamivir, peramivir and laninamivir, prevent the release of progeny virions from infected cells. Although NA inhibitors are the standard of care in most countries, their use is limited by the short therapeutic window and concern that viral resistance to these drugs may appear (Takashita et al. 2015). In the past few years, two inhibitors of the viral polymerase complex have been commercialized in certain countries, specifically the nucleoside analogue favipiravir and endonuclease inhibitor baloxavir marboxil (Jones et al. 2023).

Also HA represents an appealing drug target. To date, 18 HA subtypes (H1–H18) have been discovered for IAV and these fall into two phylogenetic groups. The H1, H2 and H5 HAs belong to group-1 whereas H3 and H7 HAs are in group-2 (Jiao et al. 2023). HA mediates two processes in the viral entry pathway: receptor binding and membrane fusion. Viral entry starts with binding of HA to sialylated glycan receptors on the host cell surface. After endocytic uptake of the virus, the low endosomal pH (pH 5.0–5.5) triggers a conformational

rearrangement in HA, which releases the hydrophobic fusion peptide from its buried position within the stem region of the HA trimer. Insertion of the fusion peptide in the endosomal membrane results in fusion of the viral and endosomal membranes, creating a fusion pore that allows release of the viral genome segments into the cytoplasm (Sempere Borau and Stertz 2021).

Arbidol (umifenovir) (Figure 1) is a broad-spectrum antiviral drug and the only inhibitor of influenza virus entry that is currently approved. It has been in the market in Russia and China since several years and is in clinical trials elsewhere (Kang et al. 2023). Besides other antiviral mechanisms, arbidol exhibits an inhibitory effect on HA-mediated fusion by preventing the conformational change of HA at low pH (Blaising et al. 2014). Crystallographic analysis of arbidol in complex with H3 and H7 HAs revealed that arbidol binds in a hydrophobic cavity within the stem of HA, functioning as a molecular glue to stabilize this trimeric protein (Kadam and Wilson 2017). This binding site in H3 HA partially overlaps with that of *tert*-butylhydroquinone (TBHQ) (Figure 1) a group-2 specific fusion inhibitor (Bodian et al. 1993; Russell et al. 2008). The HA stem region that is targeted by arbidol and TBHQ serves as a promising target for anti-influenza drug development.

In addition to arbidol and TBHQ, numerous small molecules (Figure 1) have shown promising inhibitory activity against specific HA subtypes by blocking HA-mediated fusion. These

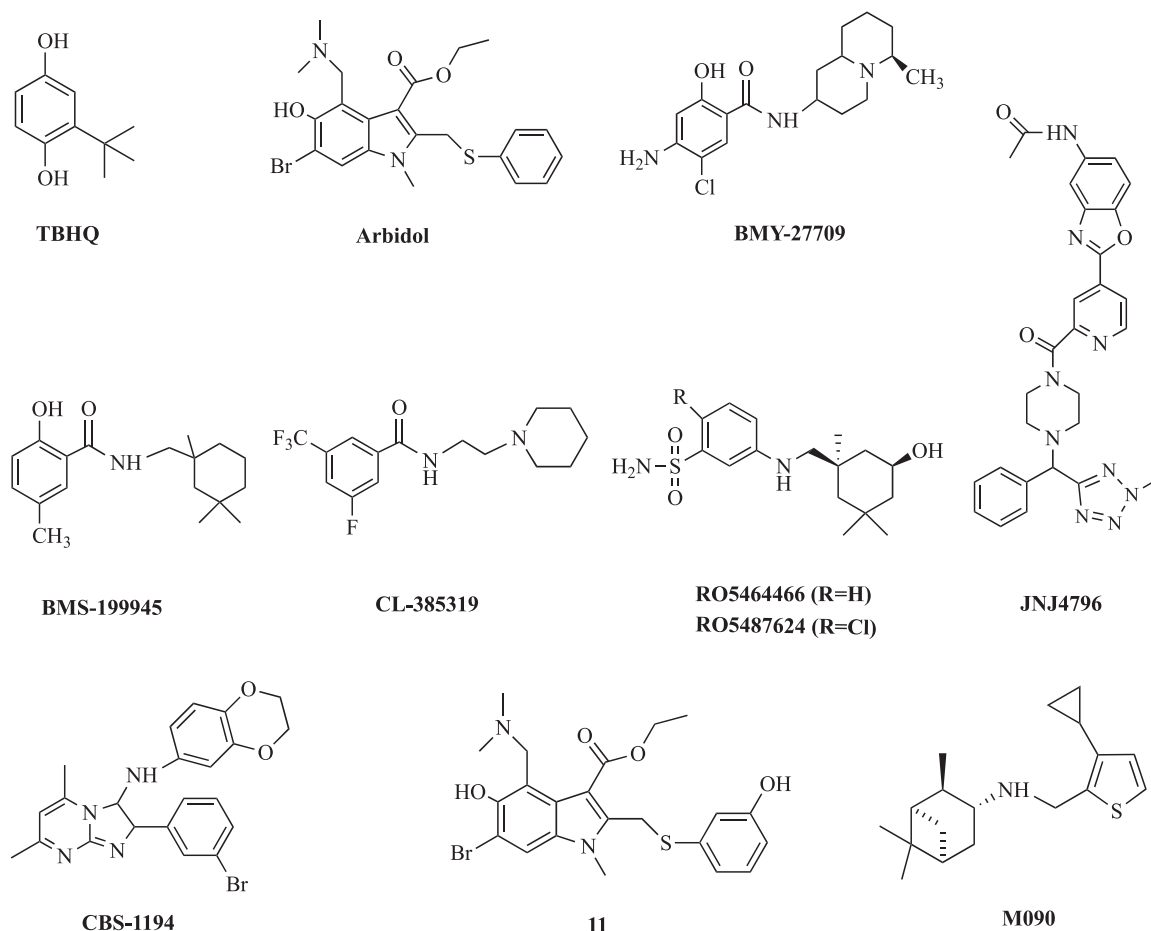


**FIGURE 1** | The structure of some compounds that inhibit HA-mediated fusion.

inhibitors function through mechanisms such as preventing HA conformational changes at low pH or binding to different regions of HA. HA fusion inhibitors can be classified into group 1-specific, group 2-specific, and broad-spectrum categories based on the HA subtypes they target (Chen et al. 2021).

Group-1 specific fusion inhibitors include compounds BMY-27709, BMS-199945, CL-385319, RO5487624, JNJ4796. Structurally related molecules, BMY-27709, BMS-199945, and CL-385319 demonstrated efficacy against influenza H1, H2, and H5 subtypes by inhibiting the low-pH-induced conformational change of the HA protein (Luo et al. 1996, 1997; Liu et al. 2011, Li et al. 2012). Benzene sulfonamide derivatives, RO5464466 and its 2-chloro analogue RO5487624 showed activity against influenza H1 subtypes and inhibited fusion by binding to HA and stabilizing its prefusion structure (Tang et al. 2011). JNJ4796, a benzylpiperazine derivative, was found to neutralize a broad range of group-1 IAVs by targeting the conserved stem region of HA (Van Dongen et al. 2019). Compared with group-1 specific inhibitors, fewer group-2 specific fusion inhibitors have been identified. CBS1194 was identified as an inhibitor of the H3 and H5 subtypes of IAV targeting the fusogenic activity of group 2 HAs by binding a region near the fusion peptide as TBHQ (Du et al. 2021). Wright et al. synthesized a series of new arbidol analogues, and compound **11**, featuring a *m*-hydroxy group on the benzene ring, exhibited enhanced affinity for both H1 and H3 HA subtypes (Wright et al. 2017). Another non-subtype-specific HA inhibitor, M090, showed in vitro activity against amantadine-resistant and oseltamivir-resistant H1N1 strains together with the H3N2 viral strain. Mechanism studies of M090 indicated that it binds to a highly conserved segment in the HA2 domain and inhibits virus-mediated membrane fusion by “locking” HA2 in its bent conformation during rearrangement. Researchers found that this domain is not absolutely group specific and may be used to design broad-spectrum agents that target both phylogenetic groups of HAs (Zhao et al. 2018).

Spiro compounds are bicyclic or polycyclic organic molecules that contain saturated rings connected through a shared atom. In 1900, Baeyer introduced the first “spiro (spirane)” as a structure consisting of two perpendicular rings, which share a

single atom to form a rigid tetrahedral center. (Baeyer 1900). Compared to planar aromatic structures, the three-dimensional nature of spirocyclic compounds, along with their positive effects on structural novelty and solubility, has contributed to their increasing prominence in drug discovery (Zheng et al. 2014; Müller et al. 2017; Hiesinger et al. 2021). Spirocyclics are also being used to tackle various challenges in drug discovery, ranging from restricting conformation to enhance target binding to modulating physicochemical and pharmacokinetic properties (Varela et al. 2025). The growing presence of spirocyclic scaffolds in recent literature suggests their broader use in the future due to their versatile characteristics.

During the past two decades, our group has engaged in the discovery of novel fusion inhibitors of IAV. We identified a series of inhibitors with spirothiazolidinone (1-thia-4-azaspiro [4.5]decane) scaffold and strong cell culture activity against influenza A/H3N2 virus. These inhibitors share a common framework, consisting of an aromatic/alicyclic ring linked to a spirothiazolidinone system via an amide bridge. Our mechanistic studies with two lead compounds, **4c** and **5f** (Figure 2), established that these spirothiazolidinone compounds prevent the conformational change of H3 HA at low pH. Selection of resistant virus combined with in silico predictions indicate that the HA binding pocket of **4c** and **5f** overlaps with that of arbidol and TBHQ (Vanderlinden et al. 2010; Cihan-Üstündağ et al. 2020). Compounds **4c** and **5f** possess an imidazo[2,1-*b*]thiazole and 5-chloro-3-methyl-1*H*-indole scaffold as the aromatic part, respectively. Via the synthesis of different series of analogues, we showed that the anti-A/H3N2 activity is maintained when the aromatic part is replaced by 1-adamantyl (Göktaş et al. 2012), 2-methylfuran-3-yl (Apaydın et al. 2021), pyridine-3-yl (Cihan-Üstündağ et al. 2022) or a substituted phenyl group, that is, *o*-hydroxyphenyl (Vanderlinden et al. 2010), 5-chloro-2-hydroxyphenyl (Göktaş et al. 2015) or 5-chloro-2-methoxyphenyl (Göktaş et al. 2019).

We here describe the synthesis, anti-IAV activity and mechanism of action of a new series of azaspiro compounds (**1a-f**, **2a-f**) comprising a 4-*tert*-butylphenyl structure as the aromatic part (Figure 2). These new analogues were designed by combining our spirothiazolidinone scaffold with the 4-*tert*-butylphenyl

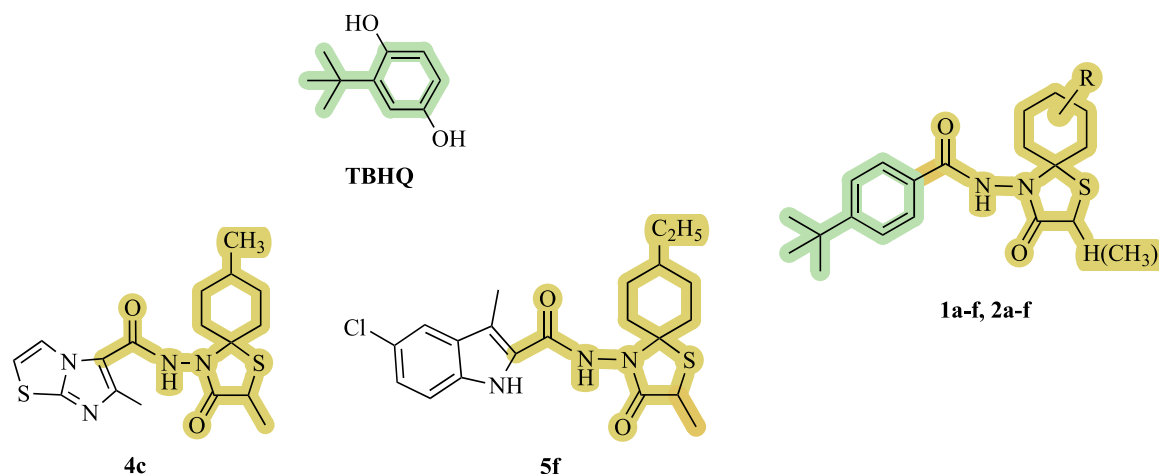


**FIGURE 2** | Chemical structures of TBHQ and spirothiazolidinone analogues, **4c** and **5f** synthesized in previous studies (Vanderlinden et al. 2010; Cihan-Üstündağ et al. 2020) and present report (**1a-f**, **2a-f**).

moiety of TBHQ. The anti-influenza virus activity was evaluated in cell-based assays using A/H1N1, A/H3N2, and IBV strains. The inhibitory effect on HA-mediated fusion was demonstrated in a polykaryon assay and molecular docking studies were conducted to predict the probable binding site of lead compound **2c** within the H3 HA protein.

## 2 | Results and Discussion

### 2.1 | Chemistry and Structural Characterization

The synthetic pathway for the preparation of the target compounds **1a-f** and **2a-f** is demonstrated in Scheme 1. The treatment of the starting material 4-*tert*-butylbenzohydrazide with an appropriate cyclic ketone and mercapto acids afforded the spirothiazolidinones (**1a-f** and **2a-f**) in a one-pot reaction. IR,  $^1\text{H}$  NMR,  $^{13}\text{C}$  NMR (APT), 2D NMR (HSQC) and microanalysis used to describe the structural characteristics of novel compounds.

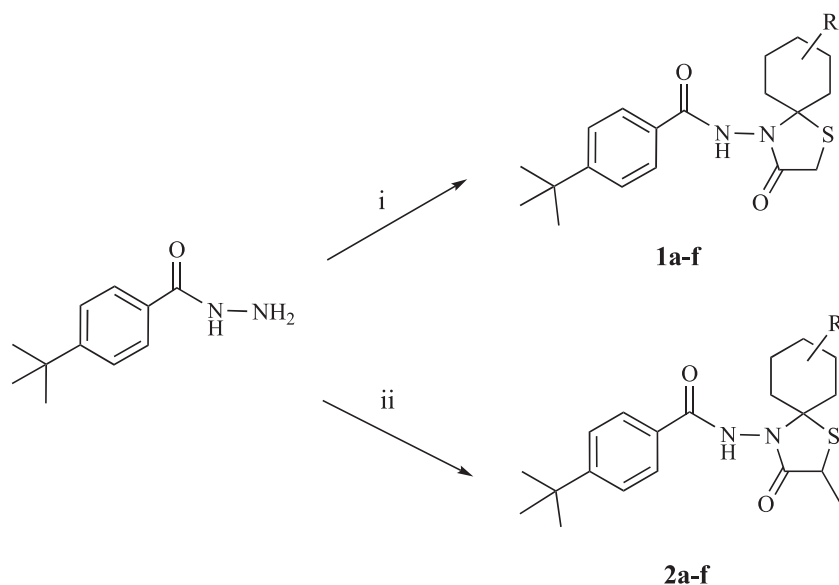
The solid phase (KBr) IR spectra of **1a-f** and **2a-f** exhibited benzamide and lactam C=O bands in the  $1654\text{--}1666\text{ cm}^{-1}$  and  $1685\text{--}1716\text{ cm}^{-1}$  regions, respectively. The shifts observed in the benzamide N-H ( $3141\text{--}3271\text{ cm}^{-1}$ ) and C=O ( $1654\text{--}1666\text{ cm}^{-1}$ ) bands when compared to that of the starting 4-*tert*-butylbenzohydrazide ( $3323$  and  $1625\text{ cm}^{-1}$ ) and the presence of additional lactam bands provided proof for the aimed cyclization. In the  $^1\text{H}$  NMR spectra of compounds **1a-f** and **2a-f**, CONH protons were observed at  $\delta$  10.43–10.50 ppm as singlets. The S-CH<sub>2</sub> (**1a-f**) protons of the newly formed thiazolidinone residue resonated at  $\delta$  3.61 ppm as singlets while S-CH (**2a-f**) protons resonated at  $\delta$  3.90–3.91 ppm as a broad/distorted doublets or quartets. The remaining proton signals of spiroalkane system were detected at  $\delta$  0.74–2.15 ppm region together with the alkyl substituents. The resonances of 4-C (CH<sub>3</sub>)<sub>3</sub> group and aromatic hydrogens were observed in the  $\delta$

1.30–1.31 ppm and  $\delta$  7.53–7.86 ppm, respectively. The splitting patterns of the aromatic H2, H6 and H3, H5 protons were in accordance with the 1,4-disubstituted aromatic ring system. Carbon assignments were established through APT experiments and 2D NMR HSQC experiment for compound **2e**. Two downfield resonances at  $\delta$  166.21–171.03 ppm region were assigned to the benzamide and lactam carbonyl groups. Observation of upfield resonances assigned to the aliphatic CH/CH<sub>2</sub> carbons and the typical spirodecane C5 resonances ( $\delta$  71.09–73.00 ppm) substantiated the formation of the expected spirothiazolidinones. The detailed spectral data of **1a-f** and **2a-f** are present in the experimental section.

### 2.2 | Anti-Influenza Virus Activity and Cytotoxicity In Cell Culture

The anti-influenza virus activity of the new spirocyclic compounds was evaluated in Madin-Darby canine kidney (MDCK) cells infected with IAV (subtype A/H1N1 or A/H3N2) or IBV. The cytopathic effect (CPE) reduction assay was based on microscopic scoring combined with the formazan-based MTS colorimetric cell viability assay. In parallel, compound cytotoxicity was determined in mock-infected cells using microscopic readout (MCC) and MTS cell viability assay (CC<sub>50</sub>) (Table 1).

Compound **2c**, featuring two methyl substituents at positions 2 and 8 of the spirocyclic ring system, displayed favorable activity against the A/H3N2 virus, with an average EC<sub>50</sub> value of  $2.4\text{ }\mu\text{M}$  (microscopic readout) or  $1.3\text{ }\mu\text{M}$  (MTS readout) (Table 1). This 2,8-dimethyl derivative showed a CC<sub>50</sub> value of  $39\text{ }\mu\text{M}$ , yielding a selectivity index (=ratio of CC<sub>50</sub> to EC<sub>50</sub>) of 30. The importance of the 8-methyl substituent is evident from the observation that compounds **2a**, **2b** and **2d-f** having no substituent, a 7-methyl group or a bulkier group at position 8, respectively, were devoid of antiviral activity. Likewise, the methyl



**SCHEME 1** | Synthesis of compounds **1a-f** and **2a-f**. Reagents and conditions: (i) (non)substituted cyclohexanone, mercaptoacetic acid, dry toluene, reflux, 5–6 h; (ii) (non)substituted cyclohexanone, 2-mercaptopropionic acid, dry toluene, reflux, 5–6 h. Compounds: **1a**, **2a**: R = H; **1b**, **2b**: R = 7-CH<sub>3</sub>; **1c**, **2c**: R = 8-CH<sub>3</sub>; **1d**, **2d**: R = 8-C<sub>2</sub>H<sub>5</sub>; **1e**, **2e**: R = 8-C<sub>3</sub>H<sub>7</sub>; **1f**, **2f**: R = C<sub>4</sub>H<sub>9</sub>.

**TABLE 1** | Anti-influenza virus activity and cytotoxicity in MDCK<sup>a</sup> cell cultures.

Compound		Antiviral EC <sub>50</sub> <sup>b</sup>						Cytotoxicity	
		A/H1N1		A/H3N2		IBV			
		CPE	MTS	CPE	MTS	CPE	MTS	MCC <sup>c</sup>	CC <sub>50</sub> <sup>d</sup>
		All values in μM							
1a	H	> 100	> 100	> 100	> 100	> 100	> 100	100	> 100
1b	7-Me	> 100	> 100	> 100	> 100	> 100	> 100	20	11
1c	8-Me	> 100	> 100	> 100	> 100	> 100	> 100	> 100	> 100
1d	8-Et	> 100	> 100	> 100	> 100	> 100	> 100	> 100	> 100
1e	8-Pr	> 100	> 100	> 100	> 100	> 100	> 100	100	> 100
1f	8- <i>t</i> -Bu	> 100	> 100	> 100	> 100	> 100	> 100	> 100	> 100
2a	H	> 100	> 100	> 100	> 100	> 100	> 100	≥ 20	92
2b	7-Me	> 100	> 100	> 100	> 100	> 100	> 100	≥ 20	78
2c	8-Me	> 100	> 100	2.4 ± 0.8	1.3 ± 0.3	> 100	> 100	≥ 20	39 ± 25
2d	8-Et	> 100	> 100	> 100	> 100	> 100	> 100	20	13
2e	8-Pr	> 100	> 100	> 100	> 100	> 100	> 100	4.0	14
2f	8- <i>t</i> -Bu	> 100	> 100	> 100	> 100	> 100	> 100	≥ 20	> 100
Oseltamivir carboxylate		0.5	0.4	0.8	0.4	0.8	0.6	> 100	> 100
Ribavirin		8.9	7.1	6.8	1.3	9.0	5.3	> 100	> 100
Rimantadine		8.0	8.7	0.7	0.8	> 200	> 200	> 200	> 200

<sup>a</sup>Madin Darby canine kidney cells.<sup>b</sup>Compound concentration producing 50% inhibition of virus-induced cytopathic effect, as determined by visual scoring of the CPE, or by the MTS cell viability assay. Virus strains: A/Ned/378/05 (A/H1N1); A/HK/7/87 (A/H3N2); B/Ned/537/05 (IBV).<sup>c</sup>Minimum compound concentration that causes a microscopically detectable alteration of normal cell morphology.<sup>d</sup>50% cytotoxic concentration based on the MTS cell viability assay.

substituent at position 2 of the spiro ring was shown to play a critical role, since the analogue of **2c** lacking this function (**1c**) was inactive. All compounds were found to be inactive against A/H1N1 virus and IBV (Table 1). The requirement of the 2-methyl substituent and positive effect of the 8-methyl substituent on anti-A/H3N2 activity, is fully consistent with our previous structure–activity relationship analysis for these spirothiazolidinone analogues (Vanderlinden et al. 2010; Göktaş et al. 2012, 2019; Cihan-Üstündağ et al. 2020; Apaydın et al. 2021). Comparing the EC<sub>50</sub> value of compound **2c** with the EC<sub>50</sub> values of previously synthesized *o*-hydroxyphenyl (Vanderlinden et al. 2010), 5-chloro-2-hydroxyphenyl (Göktaş et al. 2015) and 5-chloro-2-methoxyphenyl (Göktaş et al. 2019) derivatives, it appears that the *tert*-butyl group on the para position has a positive effect on antiviral activity. This is supported by the in silico predictions below, indicating that hydrophobic interactions of the *tert*-butyl group within the binding pocket of HA may contribute to enhance the antiviral potency.

### 2.3 | Inhibitory Effect on HA-Mediated Membrane Fusion

The polykaryon assay in HA-transfected HeLa cells was used to evaluate whether compound **2c** interferes with the membrane fusion process that occurs when HA-expressing cells are exposed to a buffer at pH 5. The EC<sub>50</sub> for inhibition of polykaryon formation by **2c** was 7.6  $\mu$ M for wild-type (WT) H3 HA

**TABLE 2** | Inhibitory effect on polykaryon formation induced by WT or mutant forms of H3 HA<sup>a</sup>.

Compound	EC <sub>50</sub> <sup>b</sup> ( $\mu$ M)		
	HA-WT pH: 5.2 <sup>c</sup>	HA-E57 <sub>2</sub> K pH: 5.2 <sup>c</sup>	HA-D112 <sub>2</sub> N pH: 5.6 <sup>c</sup>
<b>2c</b>	7.6	$\geq 28$	> 50
<b>4c</b>	1.4	12	> 50

<sup>a</sup>The two mutations in the HA2 subunit (E57<sub>2</sub>K and D112<sub>2</sub>N) were previously identified in influenza A/H3N2 viruses selected for resistance to imidazo[2,1-*b*]thiazole analogue **4c** (Vanderlinden et al. 2010). The mutations were introduced in an expression plasmid encoding the X-31 H3 HA, to perform the polykaryon assay.<sup>b</sup>EC<sub>50</sub>: compound concentration at which the number of polykaryons was 50% relative to the number observed in the no compound control. The EC<sub>50</sub> values for compound **4c** were reported earlier (Vanderlinden et al. 2010).<sup>c</sup>Fusion pH: pH at which the number of polykaryons was 50% relative to the number seen at pH 4.9. Values reported in (Vanderlinden et al. 2010).

(Table 2). We also determined the activity against two mutant forms of H3 HA (E57<sub>2</sub>K and D112<sub>2</sub>N), which were previously identified when we passaged influenza A/H3N2 virus in cell culture under selective pressure of compound **4c** (Vanderlinden et al. 2010). Compound **2c** was clearly less effective against the two HA mutants than against WT HA (Table 2). Mutation E57<sub>2</sub>K lies in the presumed binding pocket of **4c**. The involvement of residue E57<sub>2</sub> in the binding of compound **2c** was also proposed by our computer-aided docking (see below). Mutation D112<sub>2</sub>N leads to an increased fusion pH from 5.2 for WT-HA to 5.6 for the mutant, and this renders the HA insensitive to fusion



inhibitors. Also **2c** produced no inhibition of membrane fusion in cells expressing D112<sub>2</sub>N-substituted HA protein and receiving 50  $\mu$ M of compound (the highest concentration tested).

## 2.4 | Molecular Docking Studies

HA is a homotrimeric integral membrane glycoprotein consisting of a globular head domain and a stem domain. The globular head domain is formed by the HA1 subunit and contains the receptor binding site. The stem domain is primarily comprised of HA2 with some HA1 residues and contains the fusion machinery. Compared to the variable globular head domain, the stem domain is much more conserved among different HA subtypes and strains (Wu and Wilson 2020). The crystal structure of TBHQ in complex with H3 HA (PDB ID: 3EYM) shows that TBHQ binds to a hydrophobic pocket at an interface region between two HA protomers, which in turn stabilizes the HA prefusion conformation and prevents the conformational rearrangement required for membrane fusion. Arbidol binds at a similar location in the H3 HA stem (PDB ID: 5T6N) as TBHQ, but its binding site is larger and more complex (Kadam and Wilson 2017). The binding modes of TBHQ and arbidol to H3 HA are presented in Figures 3A,B. The amino acid residues interacting with TBHQ and arbidol at a distance of 4 Å are listed in Table 3. The grid determination process was greatly aided by these residues. The *tert*-butyl part of TBHQ makes hydrophobic interactions with amino acids Ile29<sub>1</sub>, Leu98<sub>2</sub>, Ala101<sub>2</sub> of protomer 1 and Glu103<sub>2</sub>, Leu99<sub>2</sub> of protomer 2. The hydroquinone part of the compound is surrounded by residues Tyr94<sub>2</sub> and Glu97<sub>2</sub> in protomer 1 and by Arg54<sub>2</sub>, Lys58<sub>2</sub>, and Glu57<sub>2</sub> in protomer 2 (Figure 3C). The binding sites of arbidol and TBHQ to H3 HA are partially overlapping. The thiophenyl group of arbidol is located at the same region lined by Arg54<sub>2</sub> and Val55<sub>2</sub> of protomer 1 and by Ile29<sub>1</sub>, Ala101<sub>2</sub> of protomer 2, as also seen with TBHQ. The nitrogen of the indole ring forms charged interactions with Glu57<sub>2</sub>, Lys58<sub>2</sub>, and Thr59<sub>2</sub> belonging to protomer 1. The hydroxyl group on the indole ring of arbidol makes polar interactions with Lys310<sub>1</sub>, Gln311<sub>1</sub>, and Asp90<sub>2</sub> of protomer 2, while hydrophobic interactions occur between the carbethoxy moiety and Trp92<sub>2</sub>, Pro293<sub>1</sub>, and Phe294<sub>1</sub> residues of protomer 1 and Glu97<sub>2</sub> residue of protomer 2 (Figure 3D).

Since compound **2c** exerts its inhibitory activity by interfering with HA-mediated fusion, computer-aided docking was performed to predict the possible binding pocket in the HA trimer. **2c** was docked into the two H3 HA crystal structures (PDB ID: 3EYM and 5T6N) using an induced fit protocol. As expected given the similarity between the two starting protein structures, the docking poses of **2c** were similar with comparable XP Gscores of around -10 kcal/mol. The binding modes of compound **2c** in the two protein structures are presented in Figures 4A,B. The amino acid residues that **2c** interacts with at a distance of 4 Å are listed in Table 3. Binding interactions of the compound at the interface in trimeric HA were evaluated through the 2D-interaction diagrams (Figures 4C,D) and common characteristics are highlighted below.

Compound **2c** mainly consists of three pharmacophore parts: a *tert*-butyl group as in TBHQ, carboxamide bridge and spirothiazolidinone ring. The *tert*-butyl groups of compound **2c** and TBHQ engage in similar hydrophobic interactions with Leu99<sub>2</sub>

of protomer 1, and Ile29<sub>1</sub> and Ala101<sub>2</sub> of protomer 2. The phenyl ring forms aromatic H-bonding between its hydrogens and Arg54<sub>2</sub> and Glu57<sub>2</sub> residues of protomer 1. Also, pi-pi stacking interactions were observed between the phenyl ring of **2c** and Lys27<sub>1</sub> of protomer 2 in the arbidol-bound structure. The carboxamide groups play a crucial role in protein-ligand connections due to the dual hydrogen bond donor and acceptor properties. Compound **2c** makes hydrogen-bonding interactions via its carboxamide groups in the TBHQ-bound structure. The nitrogen atom of its carboxamide bridge forms a hydrogen bond with the side chain carbonyl of Glu57<sub>2</sub> of protomer 1, while the lactam carbonyl of the thiazolidinone ring forms a hydrogen bond with Lys58<sub>2</sub> of protomer 1.

The spirocyclic part of compound **2c** was observed to fit within a hydrophobic cavity formed by amino acids Arg54<sub>2</sub>, Glu57<sub>2</sub>, Lys58<sub>2</sub>, Thr59<sub>2</sub>, and Trp92<sub>2</sub> of protomer 1, and Leu91<sub>2</sub>, and Tyr94<sub>2</sub> of protomer 2. In particular, amino acids Lys58<sub>2</sub>, Thr59<sub>2</sub>, and Trp92<sub>2</sub> (protomer 1) and Tyr94<sub>2</sub> (protomer 2), located in the hydrophobic pocket, enable to form ligand-receptor clashes. The position of the spirocyclic part of **2c** within this hydrophobic cavity is similar to that of TBHQ, in line with our previous findings (Vanderlinden et al. 2010; Cihan-Üstündağ et al. 2020). Several hydrophobic interactions between the surrounding residues in this region and **2c** were observed in which 2- and 8-methyl groups were also involved. An essential interaction is seen between methyl group at position 2- of the thiazolidinone ring and residues Asp90<sub>2</sub>, Ser93<sub>2</sub>, and Lys310<sub>1</sub> of protomer 2. The importance of this interaction is supported by the observation that compound **1c**, the analogue of **2c** bearing a hydrogen instead of 2-methyl group, lacks anti-A/H3N2 activity. The 8-methyl substituted cyclohexyl ring engages in hydrophobic interactions with amino acids Pro293<sub>1</sub>, Phe294<sub>1</sub>, Pro306<sub>1</sub>, and Lys307<sub>1</sub> of protomer 1 in both crystal structures.

The predicted binding mode of compound **2c** offers an explanation for the ~fourfold resistance of the E57<sub>2</sub>K-mutant H3 HA protein, as demonstrated in the polykaryon assay. Replacement of the Glu57<sub>2</sub> residue by lysine results in loss of the hydrogen bond between the glutamic acid carboxyl group and the nitrogen atom of the carboxamide bridge. Hydrophobic interactions between glutamic acid carboxyl group and the 8-methyl group on the cyclohexane ring, are further lost in E57<sub>2</sub>K-mutant H3 HA.

## 2.5 | Molecular Dynamics (MD) Studies

The binding of compound **2c** affecting the flexibility and the stability of the H3 HA protein, especially in the stem region where it is proposed to, were identified with MD simulations. The trajectories of each protein-ligand complexes with 3EYM and 5T6N were subjected to specific parameters such as RMSD and RMSF. For the ligand binding to remain stable, RMSD variations must be minimal. The RMSD values for proteins with the compound **2c** remained at ~2.1 and ~2.4 Å with a range of less than 1 Å for 3EYM and 5T6N systems, respectively. The RMSD values for the ligand compound **2c** were ~3.0 and ~3.6 Å, respectively (Figure 5). Characterizing local alterations along the protein chain is made easier with the help of the RMSF value. The protein regions that fluctuate the most during the simulation were shown by the peaks. The green vertical bars

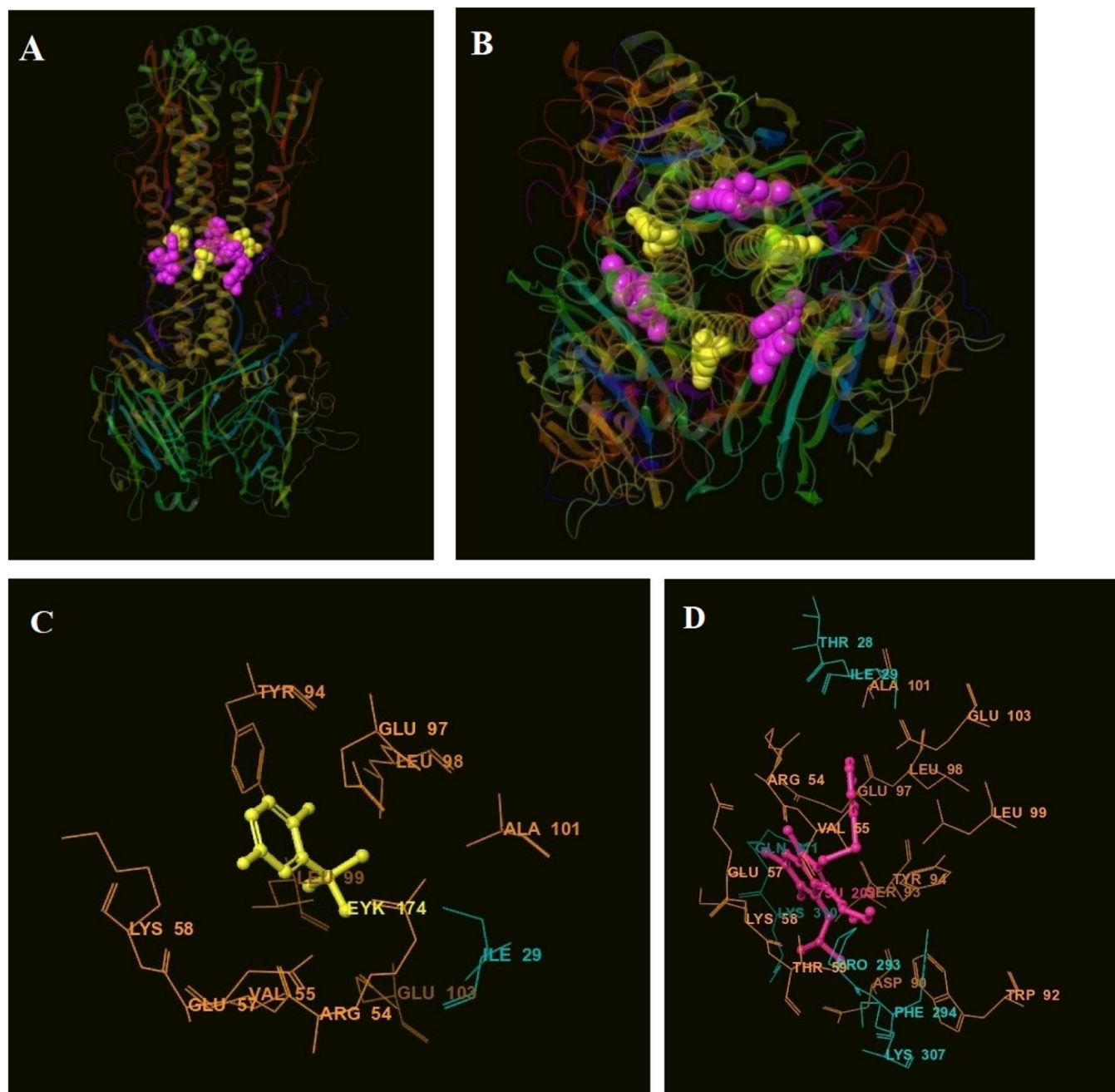


**FIGURE 3** | Reported HA binding modes for arbidol and TBHQ. (A) Vertical view of the crystal structure of H3 HA protein in complex with arbidol (in magenta) and TBHQ (in yellow). The binding pose of TBHQ (from PDB entry: 3EYM) was superimposed onto the arbidol-H3 HA cocrystal structure (PDB entry: 5T6N). (B) Top view of the crystal structure of H3 HA protein in complex with arbidol and TBHQ. (C) The binding mode of TBHQ in PDB 3EYM crystal structure. (D) The binding mode of arbidol in PDB 5T6N crystal structure. The HA1 subunits of protomer 1 and 2 are colored in blue, and the HA2 subunits are in orange. TBHQ is colored in yellow and arbidol is magenta, in structure of ball and stick.

were used to indicate the protein residues that interact with the ligand. The RMSF values for residues in the active sites were less than  $\sim 1.5$  and  $\sim 1.0$  Å, respectively (Figure 6).

Compound **2c** was observed to interact with the Arg54 amino acid of 3EYM structure with its phenyl ring via  $\pi$ -cation interaction after MD simulation (Figure 7A). And, it is observed that the compound was mainly surrounded by polar, hydrophobic and negatively charged interactions. The distances of the interactions were written on the interaction lines. In the 50 ns MD simulation time, the hydrogen bonding between amino group of

carboxamide and Arg54 amino acid was observed at a rate of 97%. Additionally, the interactions over the water molecule bridges from the carbonyl group of thiazolidinone were seen with Arg54, Glu57, and Glu97 of protomer 2 at a rate of 69%, 17%, and 11%, respectively (see the protein-ligand interaction diagram in Figure 8A). With the 5T6N structure system, it was observed that compound **2c** was surrounded by hydrophobic, polar, negatively, and positively charged interactions within the active region after MD simulation (Figure 7B). In the 50 ns MD simulation time, the water molecule bridges from the carbonyl group of thiazolidinone were observed with only Lys58 and

TABLE 3 | Interacting amino acids of H3 HA in docking structures.

Interacting amino acids of HA1 subunit			Interacting amino acids of HA2 subunit		Interacting amino acids of HA1 subunit		Interacting amino acids of HA2 subunit	
TBHQ (PDB ID: 3EYM)	Protomer 1	Ile29	Tyr94, Glu97, Leu98, Leu99, Ala101	2c (PDB ID: 3EYM)	Protomer 1	Pro293, Phe294, Pro306, Lys307	Lys51, Arg54, Val55, Ile56, Glu57, Lys58, Thr59, Asn60, Trp92, Asn95, Ala96, Leu99, Glu103	
	Protomer 2	—	Arg54, Val55, Glu57, Lys58, Leu99, Glu103		Protomer 2	Lys27, Thr28, Ile29, Thr30, Lys310, Gln311	Asp90, Leu91, Ser93, Tyr94, Glu97, Leu98, Ala101, Leu102	
Arbidol (PDB ID: 5T6N)	Protomer 1	Pro293, Phe294, Lys307	Arg54, Val55, Glu57, Lys58, Thr59, Trp92, Leu99, Glu103	2c (PDB ID: 5T6N)	Protomer 1	Pro293, Phe294, Lys307	Lys51, Arg54, Val55, Ile56, Glu57, Lys58, Thr59, Asn60, Trp92, Asn95, Leu99, Leu102, Glu103	
	Protomer 2	Thr28, Ile29, Lys310, Gln311	Asp90, Ser93, Tyr94, Glu97, Leu98, Ala101		Protomer 2	Lys27, Thr28, Ile29, Lys310, Gln311	Asp90, Leu91, Ser93, Tyr94, Glu97, Leu98, Ala101, Leu102	

Glu97 amino acids of protomer 2 at a rate of 10% and 50%, respectively. Also, the hydrogen bondings between carbonyl group of carboxamide and Arg54 (with the help of water bridge) and Lys58 amino acids were observed at a rate of 21% and 23%, respectively (see the protein-ligand interaction diagram in Figure 8C). The fraction of interactions with which residues were formed were summarized in Figures 8B,D.

### 3 | Conclusion

We here report the synthesis and antiviral evaluation of new 4-*tert*-butylphenyl-substituted spirothiazolidinones, which were easily synthesized by using one-pot cyclocondensation method. Compound **2c**, bearing methyl substitutions at positions 2- and 8- of the spiro ring displayed an EC<sub>50</sub> value against influenza A/H3N2 virus of 1.3 μM and an antiviral selectivity index of 30. Mechanistic studies including polykaryon assay and virus resistance selection with compound **2c** demonstrated that it acts as H3 HA-specific membrane fusion inhibitor. In silico studies combined with the resistance data indicated that the HA binding pocket of **2c** partially overlaps with that of arbidol and TBHQ. Compound **2c** proved inactive against E57<sub>2</sub>K-mutant H3 HA, consistent with the computer-aided predictions of its binding mode in the H3 HA trimer. The data we gained on the binding of compound **2c** to the cavity around glutamic acid-57 that is occupied by previously reported small-molecule fusion inhibitors, indicate the high relevance of this binding pocket for structure-based drug design.

### 4 | Experimental

#### 4.1 | Materials

All reagents and solvents were obtained from Merck, Fluka, and Sigma Aldrich. Melting points (m.p.) were determined on a Buchi 530 capillary melting-point apparatus in open capillaries and were uncorrected. Infrared (IR) spectra were recorded on Shimadzu IRAffinity-1 FT infrared spectrophotometer in potassium bromide pellets. <sup>1</sup>H NMR (DMSO-*d*<sub>6</sub>) spectra were run on a Varian <sup>UNITY</sup> INOVA (500-MHz) and <sup>13</sup>C NMR (APT) (DMSO-*d*<sub>6</sub>) spectra were run Bruker 500 MHz spectrophotometers. Chemical shifts were reported as δ (ppm) relative to TMS as internal standard and coupling constants (*J*) were given in hertz (Hz). ESI/MS were determined on the Finnigan LCQ Advantage Max spectrophotometer. Elemental analyses were performed on Thermo Finnigan Flash EA 1112 elemental analyzer. (\*: broad/distorted, ph.: phenyl, sp.: spirodecane).

#### 4.2 | Chemical Synthesis

##### 4.2.1 | General procedure for the synthesis of 1a-f and 2a-f

A mixture of 4-*tert*-butylbenzohydrazide (0.005 mol), an appropriate ketone (0.006 mol) and mercaptoacetic acid/2-mercaptopropionic acid (2.5 ml) was refluxed in 30 mL dry toluene for 5–6 h using a Dean–Stark apparatus. After checking with TLC that the reaction was over, excess toluene was



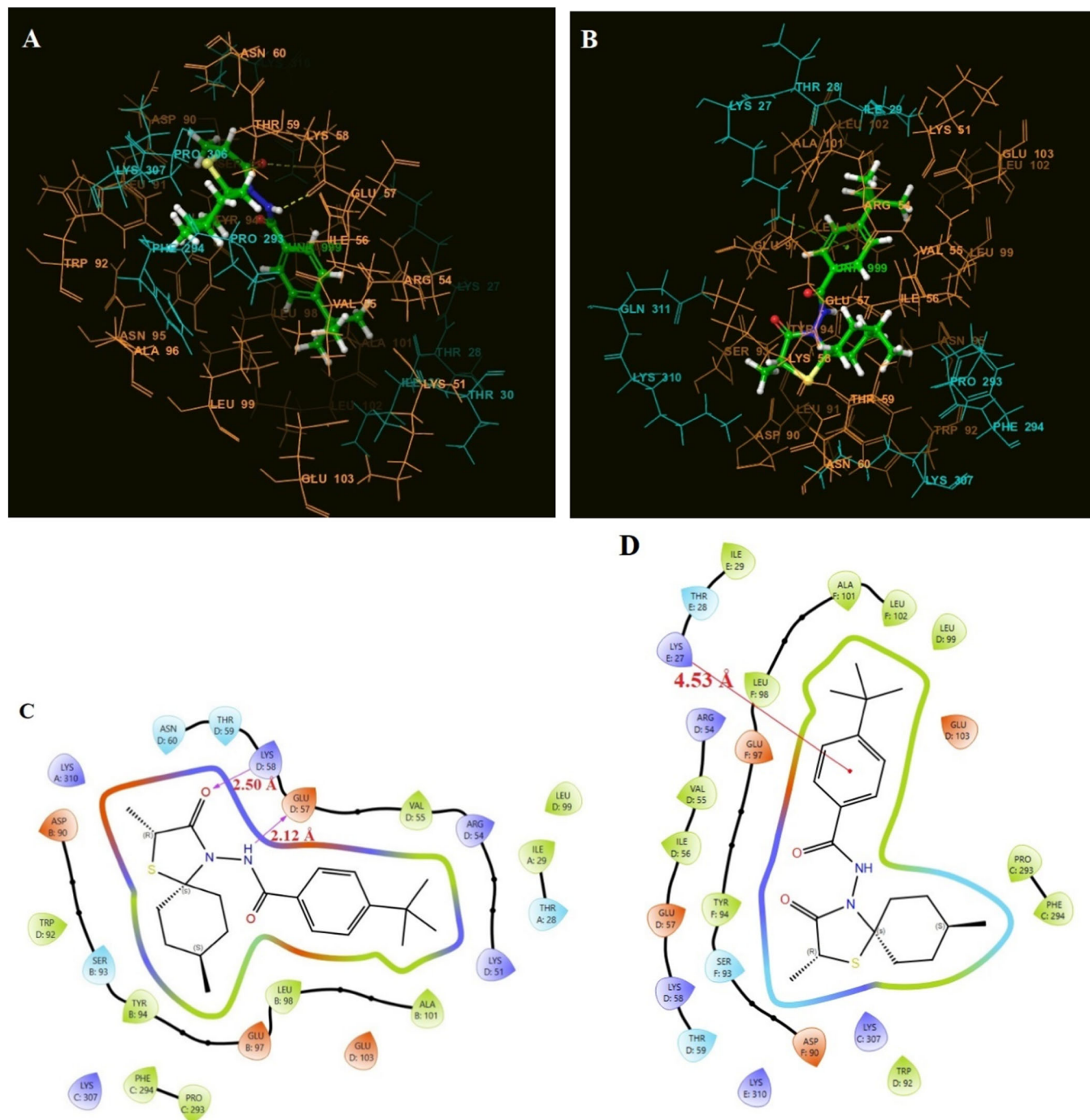


**FIGURE 4** | Predicted H3 HA binding modes (A, B) and 2D- interaction diagrams (C, D) of compound 2c. The molecule was docked into the two H3 HA structures: PDB 3EYM (A, C) and PDB 5T6N (B, D). In (A, B) the molecule is in ball and stick representation. The HA1 subunits of protomer 1 and 2 are colored in blue, and the HA2 subunits are in orange. In (C, D) the colored lines around the compound visualize interactions according to colors: green for hydrophobic, turquoise for polar, blue for positively charged, and red for negatively charged.

evaporated in vacuo. The residue was quenched with saturated  $\text{NaHCO}_3$  until  $\text{CO}_2$  evolution ceased. The solid was filtered, washed with water, and recrystallized from ethanol.

#### 4.2.2 | 4-(*tert*-Butyl)-N-(3-oxo-1-thia-4-azaspiro[4.5]decan-4-yl)benzamide (1a)

Yield: 33.72%, mp: 215.2-216.2°C; IR (KBr)  $\nu_{\text{max}}$  ( $\text{cm}^{-1}$ ): 3271 (N-H); 1714, 1660 (C=O);  $^1\text{H-NMR}$  (DMSO- $d_6$ /500 MHz): 1.02-

1.09 (1H, m,  $\text{CH}_2$ -sp.), 1.31 (9H, s, 4- $\text{C}(\text{CH}_3)_3$ -sp.), 1.40-1.55 (3H, m,  $\text{CH}_2$ -sp.), 1.71-2.05 (6H, m,  $\text{CH}_2$ -sp.), 3.61 (2H, s,  $\text{H}_2$ -sp.), 7.53 (2H, d,  $J = 8.8$  Hz, H3,H5-ph.), 7.85 (2H, d,  $J = 8.8$  Hz, H2,H6-ph.), 10.44 (1H, s, NH).  $^{13}\text{C-NMR}$  (APT) (DMSO- $d_6$ /125 MHz): 23.38, 24.45 ( $\text{CH}_2$ -sp.), 28.41 (C2-sp.), 31.35 (4- $\text{C}(\text{CH}_3)_3$ -ph.), 35.20 (4- $\text{C}(\text{CH}_3)_3$ -ph.), 72.85 (C5-sp.), 125.75 (C3,C5-ph.), 128.08 (C2,C6-ph.), 129.70 (C1-ph.), 155.62 (C4-ph.), 166.32 (CONH), 168.16 (CO-sp.). Anal. calcd. for  $\text{C}_{19}\text{H}_{26}\text{N}_2\text{O}_2\text{S}$  (346.49) C: 65.86; H:7.56; N:8.09. Found C: 65.89; H:7.86; N:7.70.

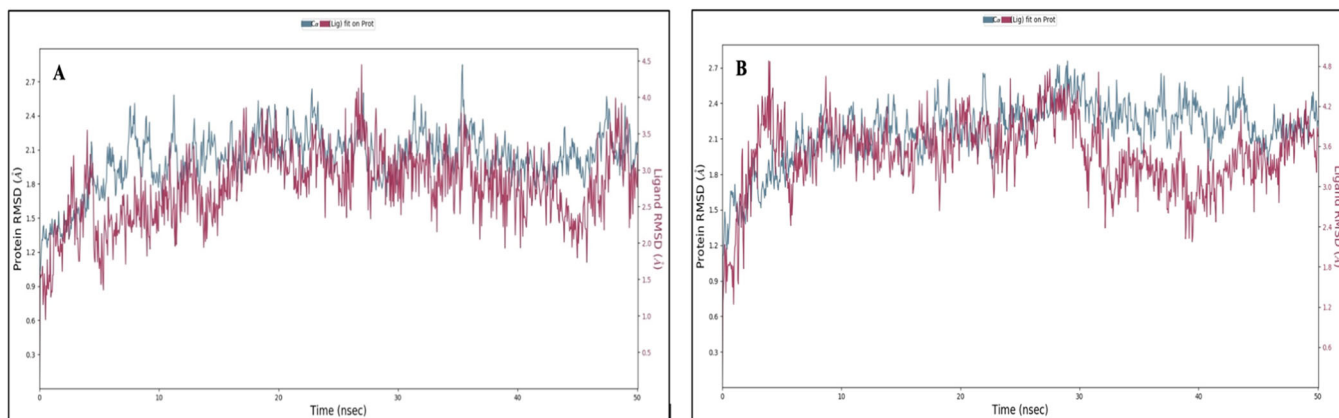


**FIGURE 5** | The RMSD graphic for the protein and ligand 2c during the MD simulation (A for PDB ID: 3EYM, B for PDB ID: 5T6N).

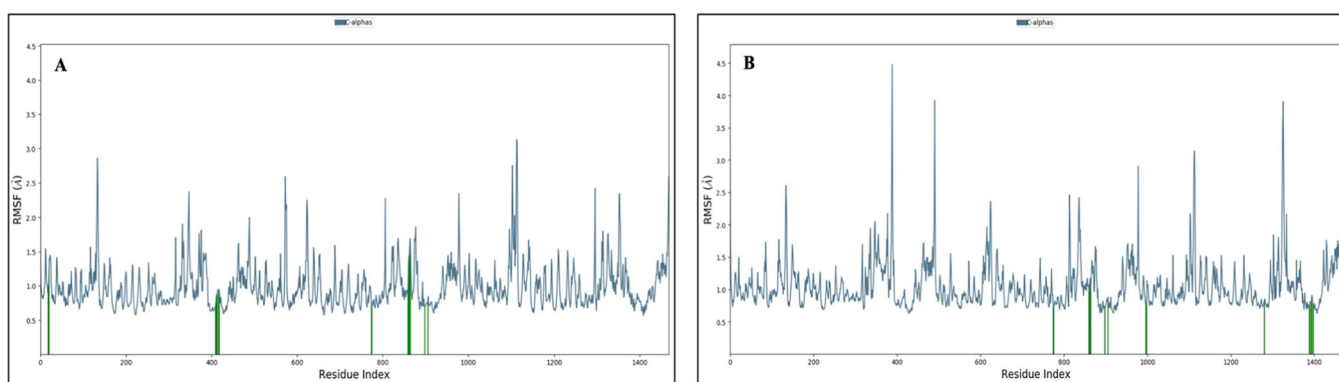


**FIGURE 6** | The RMSF graphic for the protein during the MD simulation with the compound 2c (A for PDB ID: 3EYM, B for PDB ID: 5T6N).

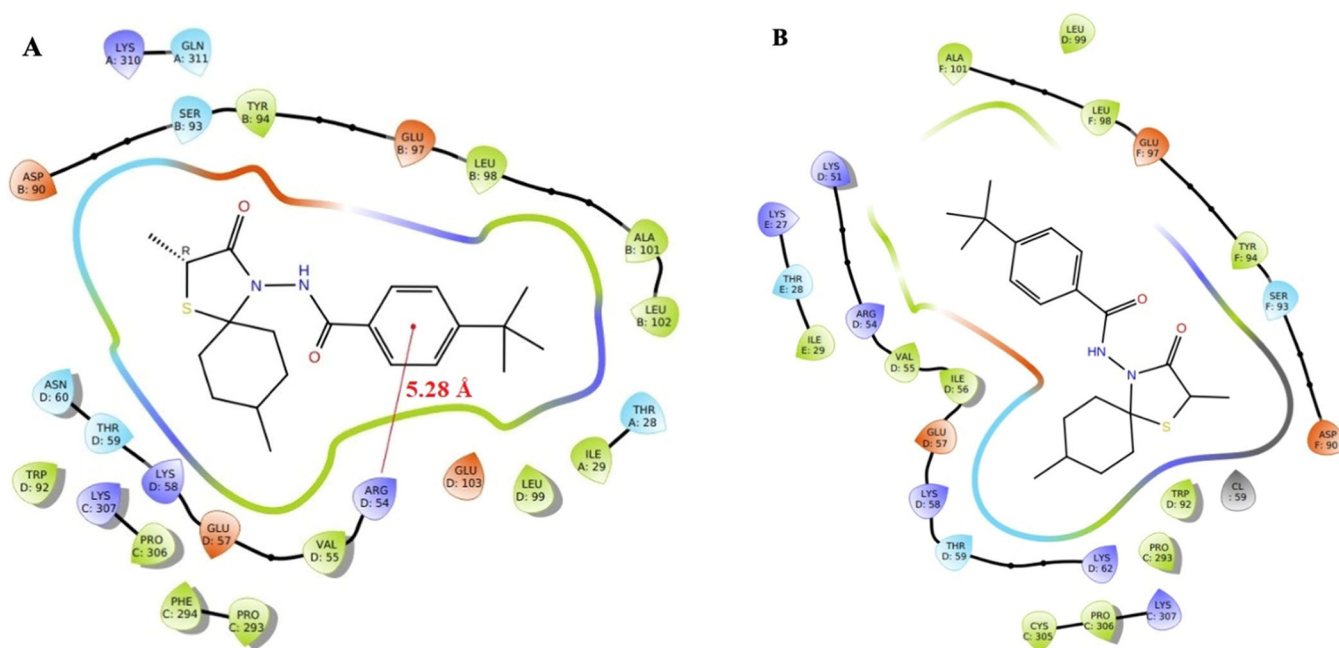


**FIGURE 7** | 2D-interaction diagram of compound 2c at active site on H3 HA after MD simulation (A for PDB ID: 3EYM, B for PDB ID: 5T6N).



#### 4.2.6 | 4-(*tert*-Butyl)-*N*-(3-oxo-8-propyl-1-thia-4-azaspiro[4.5]decan-4-yl)benzamide (1e)

Yield: 72.16%. mp: 242–243°C; IR (KBr)  $\nu_{\max}$  (cm<sup>-1</sup>): 3200 (N-H); 1709, 1661 (C=O); <sup>1</sup>H-NMR (DMSO-*d*<sub>6</sub>/500 MHz): 0.84 (3H, t, *J* = 7.5 Hz, 8-CH<sub>2</sub>CH<sub>2</sub>CH<sub>3</sub>-sp.), 1.12–1.31 (7H, m, CH/CH<sub>2</sub>-sp., 8-CH<sub>2</sub>CH<sub>2</sub>CH<sub>3</sub>-sp.), 1.31 (9H, s, 4-C(CH<sub>3</sub>)<sub>3</sub>-ph.), 1.60–2.05 (6H, m, CH/CH<sub>2</sub>-sp.), 3.61 (2H, s, H2-sp.) 7.53 (2H, d, *J* = 8.8 Hz, H3,H5-ph.), 7.85 (2H, d, *J* = 8.8 Hz, H2,H6-ph.), 10.46 (1H, s, NH). <sup>13</sup>C-NMR (APT) (DMSO-*d*<sub>6</sub>/125 MHz): 14.59 (8-CH<sub>2</sub>CH<sub>2</sub>CH<sub>3</sub>-sp.), 19.94 (8-CH<sub>2</sub>CH<sub>2</sub>CH<sub>3</sub>-sp.), 28.41 (C2-sp.), 29.81 (CH<sub>2</sub>-sp., 8-CH<sub>2</sub>CH<sub>2</sub>CH<sub>3</sub>), 31.35 (4-C(CH<sub>3</sub>)<sub>3</sub>-ph.), 35.20 (4-C(CH<sub>3</sub>)<sub>3</sub>-ph.), 35.45 (C8-sp.), 38.83 (CH<sub>2</sub>-sp., 8-CH<sub>2</sub>CH<sub>2</sub>CH<sub>3</sub>), 72.99 (C5-sp.), 125.73 (C3,C5-ph.), 128.08 (C2,C6-ph.), 129.70 (C1-ph.), 155.60 (C4-ph.), 166.31 (CONH), 168.19 (CO-sp.). Anal. calcd. for C<sub>22</sub>H<sub>32</sub>N<sub>2</sub>O<sub>2</sub>S (388.57) C:68.00; H:8.30; N:7.21. Found: C:67.89; H:8.23; N:7.12.

#### 4.2.7 | 4-(*tert*-Butyl)-*N*-(8-(*tert*-butyl)-3-oxo-1-thia-4-azaspiro[4.5]decan-4-yl)benzamide (1f)

Yield: 22%. mp: 179–181°C; IR (KBr)  $\nu_{\max}$  (cm<sup>-1</sup>): 3155 (N-H); 1689, 1663 (C=O); <sup>1</sup>H-NMR (DMSO-*d*<sub>6</sub>/500 MHz): 0.81 (9H, s, 8-C(CH<sub>3</sub>)<sub>3</sub>-sp.); 0.83–1.26 (3H, m, CH/CH<sub>2</sub>-sp.), 1.31 (9H, s, 4-C(CH<sub>3</sub>)<sub>3</sub>-ph.), 1.47–2.15 (6H, m, CH/CH<sub>2</sub>-sp.), 3.61 (2H, s, H2-sp.), 7.53 (2H, d, *J* = 8.3 Hz, H3,H5-ph.), 7.85 (2H, d, *J* = 8.3 Hz, H2, H6-ph.), 10.45 (1H, s, NH). <sup>13</sup>C-NMR (APT) (DMSO-*d*<sub>6</sub>/125 MHz): 24.19 (CH<sub>2</sub>-sp.), 27.75 (8-C(CH<sub>3</sub>)<sub>3</sub>-sp.), 28.40 (C2-sp.), 31.35 (4-C(CH<sub>3</sub>)<sub>3</sub>-ph.), 32.39 (8-C(CH<sub>3</sub>)<sub>3</sub>-sp.), 35.20 (4-C(CH<sub>3</sub>)<sub>3</sub>-ph.), 46.17 (C8-sp.), 72.86 (C5-sp.), 125.73 (C3,C5-ph.), 128.08 (C2,C6-ph.), 129.69 (C1-ph.), 155.60 (C4-ph.), 166.29 (CONH), 168.22 (CO-sp.). Anal. calcd. for C<sub>23</sub>H<sub>34</sub>NO<sub>2</sub>S.H<sub>2</sub>O (420.24) C:65.68; H:8.63; N:6.66. Found: C:65.34; H:8.42; N:6.69.

#### 4.2.8 | 4-(*tert*-Butyl)-*N*-(2-methyl-3-oxo-1-thia-4-azaspiro[4.5]decan-4-yl)benzamide (2a)

Yield: 59.72%. mp: 224–226.5°C; IR (KBr)  $\nu_{\max}$  (cm<sup>-1</sup>): 3240 (N-H); 1716, 1662 (C=O); <sup>1</sup>H-NMR (DMSO-*d*<sub>6</sub>/500 MHz): 1.02–1.04 (1H, m, CH<sub>2</sub>-sp.), 1.30 (9H, s, 4-C(CH<sub>3</sub>)<sub>3</sub>-ph.), 1.44 (3H, d, *J* = 6.8 Hz, 2-CH<sub>3</sub>-sp.), 1.55–1.55 (3H, m, CH<sub>2</sub>-sp.), 1.71–2.05 (6H, m, CH<sub>2</sub>-sp.), 3.91 (1H, d\*, *J* = 6.3 Hz, H2-sp.), 7.53 (2H, d, *J* = 8.3 Hz, H3,H5-ph.), 7.86 (2H, d, *J* = 8.3 Hz, H2,H6-ph.), 10.50 (1H, s, NH-disappeared on D<sub>2</sub>O exchange). <sup>13</sup>C-NMR (APT) (DMSO-*d*<sub>6</sub>/125 MHz): 23.47, 23.92, 24.66 (CH<sub>2</sub>-sp.), 31.58 (4-C(CH<sub>3</sub>)<sub>3</sub>-ph.), 35.40 (4-C(CH<sub>3</sub>)<sub>3</sub>-ph.), 37.51 (C2-sp.), 71.72 (C5-sp.), 125.97 (C3,C5-ph.), 128.38 (C2,C6-ph.), 129.92 (C1-ph.), 155.83 (C4-ph.), 166.47 (CONH), 171.00 (CO-sp.). Anal. calcd. for C<sub>20</sub>H<sub>28</sub>N<sub>2</sub>O<sub>2</sub>S (360.52) C: 66.63; H: 7.83; N: 7.77. Found C:66.53; H: 8.46; N: 7.84.

#### 4.2.9 | 4-(*tert*-Butyl)-*N*-(2,7-dimethyl-3-oxo-1-thia-4-azaspiro[4.5]decan-4-yl)benzamide (2b)

Yield: 19,78%. mp: 220.5–222.5°C; IR  $\nu_{\max}$  (cm<sup>-1</sup>): 3230 (N-H); 1714, 1666 (C=O); <sup>1</sup>H-NMR (DMSO-*d*<sub>6</sub>/500 MHz): 0.74 (1H, q\*, *J* = 11.0 Hz, CH/CH<sub>2</sub>-sp.), 0.87 (3H, s, 7-CH<sub>3</sub>-sp.), 1.30 (9H, s,

4-C(CH<sub>3</sub>)<sub>3</sub>-ph.), 1.43 (3H, d, *J* = 6.9 Hz, 2-CH<sub>3</sub>-sp.), 1.49–1.80 (8H, m, CH/CH<sub>2</sub>-sp.), 3.90 (1H, d\*, *J* = 6.8 Hz, H2-sp.), 7.53 (2H, d, *J* = 8.3 Hz, H3,H5-ph.), 7.85 (2H, d, *J* = 8.3 Hz, H2,H6-ph.), 10.45 (1H, s, NH). <sup>13</sup>C-NMR (APT) (DMSO-*d*<sub>6</sub>/125 MHz): 22.45, 22.60 (7-CH<sub>3</sub>-sp., 2-CH<sub>3</sub>-sp.), 23.20 (CH<sub>2</sub>-sp.), 29.90 (C7-sp.), 31.36 (4-C(CH<sub>3</sub>)<sub>3</sub>-ph.), 33.17 (CH<sub>2</sub>-sp.), 35.19 (4-C(CH<sub>3</sub>)<sub>3</sub>-ph.), 37.34 (C2-sp.), 71.49 (C5-sp.), 125.72 (C3,C5-ph.), 128.08 (C2,C6-ph.), 129.86 (C1-ph.), 155.52 (C4-ph.), 166.26 (CONH), 170.59 (CO-sp.). Anal. calcd. for C<sub>21</sub>H<sub>30</sub>N<sub>2</sub>O<sub>2</sub>S (374.54) C: 67.34; H: 8.07; N: 7.48. Found C:67.25; H: 8.17; N: 7.64.

#### 4.2.10 | 4-(*tert*-Butyl)-*N*-(2,8-dimethyl-3-oxo-1-thia-4-azaspiro[4.5]decan-4-yl)benzamide (2c)

Yield: 38.21%. mp: 139–141.5°C; IR  $\nu_{\max}$ (cm<sup>-1</sup>): 3431, 3419 (O-H), 3151, 3141 (N-H); 1685, 1660 (C=O); <sup>1</sup>H-NMR (DMSO-*d*<sub>6</sub>/500 MHz): 0.85 (3H, d, *J* = 5.9 Hz, 8-CH<sub>3</sub>-sp.), 1.09–1.27 (3H, m, CH/CH<sub>2</sub>-sp.), 1.30 (9H, s, 4-C(CH<sub>3</sub>)<sub>3</sub>-ph.), 1.44 (3H, d, *J* = 6.8 Hz, 2-CH<sub>3</sub>-sp.), 1.67–2.05 (6H, m, CH/CH<sub>2</sub>-sp.), 3.91 (1H, d\*, *J* = 6.3 Hz, H2-sp.), 7.53 (2H, d, *J* = 8.3 Hz, H3,H5-ph.), 7.85 (2H, d, *J* = 8.3 Hz, H2,H6-ph.), 10.49 (1H, s, NH). <sup>13</sup>C-NMR (APT) (DMSO-*d*<sub>6</sub>/125 MHz): 22.34 (8-CH<sub>3</sub>-sp.), 30.92 (C8-sp.), 31.35 (4-C(CH<sub>3</sub>)<sub>3</sub>-ph.), 31.70, 32.18 (CH<sub>2</sub>-sp.), 35.40 (4-C(CH<sub>3</sub>)<sub>3</sub>-ph.), 37.26 (C2-sp.), 71.34 (C5-sp.), 125.76 (C3,C5-ph.), 128.05 (C2,C6-ph.), 129.67 (C1-ph.), 155.62 (C4-ph.), 166.21 (CONH), 170.83 (CO-sp.). (ESI+) MS *m/z* (%): 374.9 ([*M* + *H*]<sup>+</sup>, 100). Anal. calcd. for C<sub>21</sub>H<sub>30</sub>N<sub>2</sub>O<sub>2</sub>S.H<sub>2</sub>O (392.56) C: 64.25; H: 8.22; N: 7.14. Found C:64.27; H: 9.18; N: 6.94.

#### 4.2.11 | 4-(*tert*-Butyl)-*N*-(8-ethyl-2-methyl-3-oxo-1-thia-4-azaspiro[4.5]decan-4-yl)benzamide (2d)

Yield: 14.28%. mp: 135–136.5°C; IR  $\nu_{\max}$  (cm<sup>-1</sup>): 3415 (O-H), 3145 (N-H); 1685, 1662 (C=O); <sup>1</sup>H-NMR (DMSO-*d*<sub>6</sub>/500 MHz): 0.82 (3H, t, *J* = 7.8 Hz, 8-CH<sub>2</sub>CH<sub>3</sub>-sp.), 1.05–1.18 (5H, m, CH/CH<sub>2</sub>-sp., 8-CH<sub>2</sub>CH<sub>3</sub>-sp.), 1.30 (9H, s, 4-C(CH<sub>3</sub>)<sub>3</sub>-ph.), 1.44 (3H, d, *J* = 6.8 Hz, 2-CH<sub>3</sub>-sp.), 1.67–2.01 (6H, m, CH/CH<sub>2</sub>-sp.), 3.91 (1H, q, *J* = 6.3 Hz, H2-sp.), 7.53 (2H, d, *J* = 8.3 Hz, H3,H5-ph.), 7.85 (2H, d, *J* = 8.3 Hz, H2,H6-ph.), 10.49 (1H, s, NH). <sup>13</sup>C-NMR (APT) (DMSO-*d*<sub>6</sub>/125 MHz): 11.81 (8-CH<sub>2</sub>CH<sub>3</sub>-sp.), 20.32 (2-CH<sub>3</sub>-sp.), 29.22, 29.27, 29.72 (CH<sub>2</sub>-sp., 8-CH<sub>2</sub>CH<sub>3</sub>-sp.), 31.36 (4-C(CH<sub>3</sub>)<sub>3</sub>-ph.), 35.19 (4-C(CH<sub>3</sub>)<sub>3</sub>-ph.), 37.30, 37.51 (C2-sp., C8-sp.), 71.66 (C5-sp.), 125.72 (C3,C5-ph.), 128.05 (C2,C6-ph.), 129.88 (C1-ph.), 155.51 (C4-ph.), 166.29 (CONH), 170.71 (CO-sp.). Anal. calcd. for C<sub>22</sub>H<sub>32</sub>N<sub>2</sub>O<sub>2</sub>S.H<sub>2</sub>O (406.58) C: 64.99; H: 8.43; N: 6.89. Found C:65.04; H: 8.12; N: 7.05.

#### 4.2.12 | 4-(*tert*-Butyl)-*N*-(2-methyl-3-oxo-8-propyl-1-thia-4-azaspiro[4.5]decan-4-yl)benzamide (2e)

Yield: 44.71%. mp: 201–202.5°C; IR  $\nu_{\max}$  (cm<sup>-1</sup>): 3261 (N-H); 1716, 1662 (C=O); <sup>1</sup>H-NMR (DMSO-*d*<sub>6</sub>/500 MHz): 0.83 (3H, t, *J* = 7.3 Hz, 8-CH<sub>2</sub>CH<sub>2</sub>CH<sub>3</sub>-sp.), 1.04–1.17 (5H, m, CH/CH<sub>2</sub>-sp., 8-CH<sub>2</sub>CH<sub>2</sub>CH<sub>3</sub>-sp.), 1.23–1.28 (2H, m, 8-CH<sub>2</sub>CH<sub>2</sub>CH<sub>3</sub>-sp.), 1.30 (9H, s, 4-C(CH<sub>3</sub>)<sub>3</sub>-ph.), 1.44 (3H, d, *J* = 6.8 Hz, 2-CH<sub>3</sub>-sp.), 1.73–2.15 (6H, m, CH/CH<sub>2</sub>-sp.), 3.91 (1H, d\*, *J* = 6.4 Hz, H2-sp.), 7.53 (2H, d, *J* = 8.3 Hz, H3,H5-ph.), 7.86 (2H, d, *J* = 8.3 Hz, H2,H6-



ph.), 10.49 (1H, s, NH). <sup>13</sup>C-NMR (HSQC) (125 MHz) (DMSO-*d*<sub>6</sub>/TMS): 14.79 (8-CH<sub>2</sub>CH<sub>2</sub>C(CH<sub>3</sub>)<sub>3</sub>-sp.), 20.14 (2-CH<sub>3</sub>-sp., 8-CH<sub>2</sub>CH<sub>2</sub>CH<sub>3</sub>-sp.), 29.88, 30.33 (CH<sub>2</sub>-sp.), 31.57 (4-C(CH<sub>3</sub>)<sub>3</sub>-ph.), 35.42 (4-C(CH<sub>3</sub>)<sub>3</sub>-ph.), 35.66 (C8-sp.), 37.34 (CH<sub>2</sub>-sp.), 37.43 (C2-sp.), 39.07 (8-CH<sub>2</sub>CH<sub>2</sub>CH<sub>3</sub>-sp.), 71.86 (C5-sp.), 125.95 (C3,C5-ph.), 128.38 (C2,C6-ph.), 129.94 (C1-ph.), 155.83 (C4-ph.), 166.47 (CONH), 171.03 (CO-sp.). Anal. calcd. for C<sub>23</sub>H<sub>30</sub>N<sub>2</sub>O<sub>2</sub>S (402.59) C: 68.62; H: 8.51; N: 6.72. Found C:68.67; H: 8.83; N: 6.44.

#### 4.2.13 | 4-(*tert*-Butyl)-*N*-(8-(*tert*-butyl)-2-methyl-3-oxo-1-thia-4-azaspiro[4.5]decan-4-yl)benzamide (2f)

Yield: 47.86%. mp: 159–161°C. IR  $\nu_{\text{max}}$  (cm<sup>-1</sup>): 3412 (O-H), 3151 (N-H); 1689, 1654 (C=O); <sup>1</sup>H-NMR (DMSO-*d*<sub>6</sub>/500 MHz): 0.81 (9H, s, 8-C(CH<sub>3</sub>)<sub>3</sub>-sp.), 0.83–0.93 (1H, m, CH/CH<sub>2</sub>-sp.), 1.17–1.26 (2H, m, CH/CH<sub>2</sub>-sp.), 1.30 (9H, s, 4-C(CH<sub>3</sub>)<sub>3</sub>-ph.), 1.44 (3H, d, *J* = 6.8 Hz, 2-CH<sub>3</sub>-sp.), 1.73–2.15 (6H, m, CH/CH<sub>2</sub>-sp.), 3.91 (1H, q, *J* = 5.9 Hz, H2-sp.), 7.53 (2H, d, *J* = 8.3 Hz, H3,H5-ph.), 7.85 (2H, d, *J* = 8.3 Hz, H2,H6-ph.), 10.50 (1H, s, NH). <sup>13</sup>C-NMR (APT) (DMSO-*d*<sub>6</sub>/125 MHz): 20.35 (2-CH<sub>3</sub>), 24.03, 24.46 (CH<sub>2</sub>-sp.), 27.74 (8-C(CH<sub>3</sub>)<sub>3</sub>-sp.), 31.35 (4-C(CH<sub>3</sub>)<sub>3</sub>-ph.), 32.39 (8-C(CH<sub>3</sub>)<sub>3</sub>-sp.), 35.20 (4-C(CH<sub>3</sub>)<sub>3</sub>-ph.), 37.30 (C2-sp.), 46.11 (C8-sp.), 71.52 (C5-sp.), 125.74 (C3,C5-ph.), 128.06 (C2,C6-ph.), 129.67 (C1-ph.), 155.61 (C4-ph.), 166.21 (CONH), 170.86 (CO-sp.). (ESI+) MS *m/z* (%): 417.2 ([*M* + *H*]<sup>+</sup>, 100). Anal. calcd. for C<sub>24</sub>H<sub>36</sub>N<sub>2</sub>O<sub>2</sub>S.H<sub>2</sub>O (434.64) C: 66.32; H: 8.81; N: 6.45. Found C:66.27; H: 8.33; N: 6.62.

#### 4.3 | Antiviral Assay

The CPE reduction assay for IAV and IBV was reported in full detail elsewhere [Vanderlinden et al. 2010]. Briefly, MDCK cells were seeded in 96-well plates and, on the next day, virus was added [A/H1N1 (strain A/Ned/378/05), A/H3N2 (A/HK/7/87) or IBV (B/Ned/537/05)] at a multiplicity of infection of 100 CCID<sub>50</sub> (50% cell culture infective dose) per well. At the same time, the compounds were added at serial dilutions. After 4 days incubation at 35°C, the compounds' protective effect against viral CPE as well as their cytotoxicity were assessed by microscopy and the colorimetric MTS cell viability assay (CellTiter 96 AQueous One Solution Cell Proliferation Assay from Promega). Antiviral activity was expressed as the 50% effective concentration (EC<sub>50</sub>), whereas cytotoxicity was defined as MCC (minimal cytotoxic concentration, based on microscopy) or CC<sub>50</sub> (50% cytotoxic concentration, assessed by the MTS assay). The formulas used to calculate these parameters were published elsewhere (Vrijens et al. 2019).

#### 4.4 | Polykaryon Assay

The polykaryon assay (see [Vanderlinden et al. 2010] for all details) was performed with pCAGEN plasmids expressing wild-type or mutant (E57<sub>2</sub>K and D112<sub>2</sub>N) forms of A/X-31 H3 HA. HeLa cells were seeded into 12-well plates and transfected with HA plasmid using Fugene 6 reagent (Promega). Two days later, the cells were briefly exposed to TPCK-treated trypsin to

activate the HA on the cell surface. After two rinses with PBS containing Ca<sup>2+</sup> and Mg<sup>2+</sup> (PBS-CM), the cells were pre-incubated with compound during 15 min. Next, they were exposed to acidic buffer (PBS-CM adapted to pH 5) containing the same concentration of compound, and incubated for exactly 15 min at 37°C. After two rinses with PBS-CM, medium with 10% fetal calf serum was added. Three hours later, the cells were fixated with ethanol and stained with Giemsa. Microscopy at x200 magnification was conducted to count the number of polykaryons (containing five or more nuclei) in four randomly selected microscopic fields.

#### 4.5 | Molecular Docking Studies

All molecular docking process was performed on Schrödinger Small Molecule Drug Discovery Suite program (v.2022-1, Maestro, Schrödinger, Limited Liability Company, New York, 2022). The chosen compound was drawn by the 2D Sketcher application in Maestro, energy minimization was done at pH 7.0 according to OPLS4 technic, and the LigPrep application was used to create the 3D ligand structure. The protein and grid preparation procedures were carried out according to the literature (Cihan-Üstündağ et al. 2020). The crystal structures for H3 HA were procured with the pdb codes 3EYM (strain A/Aichi/2/1968 H3N2) and 5T6N (strain A/Hong Kong/1/1968 H3N2 and strain A/Northern Territory/60/1968 H3N2) from Protein Data Bank database (PDB). 3EYM (2.8 Å) includes the influenza virus haemagglutinin in complex with 2-*tert*-butylbenzene-1,4-diol (TBHQ) (Russell et al. 2008) and 5T6N (2.54 Å) contains the influenza virus HA in complex with the influenza virus fusion inhibitor drug, arbidol (ethyl 6-bromo-4-[(dimethylamino)methyl]-5-hydroxy-1-methyl-2-[(phenylsulfanyl)methyl]-1*H*-indole-3-carboxylate) (Kadam and Wilson 2017). Before docking, crystal structures of the proteins were prepared by removing ligands from the respective hydrophobic pockets and applying the Protein Preparation Wizard Module of Schrodinger Software Suite. Hydrogen addition at pH 7.0, optimization, and energy minimization were performed. The grid was generated by taking the centroid of ligands with Receptor Grid Generation application. The three chains in the trimer are labeled A, C, and E (HA1) and B, D, and F (HA2). The subscript number 1 or 2 after the amino acid residue number indicates their location in the HA1 or HA2 subunit, respectively. The grid includes Arg54<sub>2</sub>, Val55<sub>2</sub>, and Glu57<sub>2</sub> of monomer 1 and Tyr94<sub>2</sub>, Glu97<sub>2</sub>, and Leu99<sub>2</sub> of monomer 2 for 5T6N.pdb. The grid for 3EYM.pdb was also detected with the same residues. The prepared ligand was docked into the grids with standard protocol and extra precision (XP) method according to the Induced Fit Docking (IFD) protocol. The poses were ranked based on XP G-scores and examined for protein-ligand interactions.

#### 4.6 | MD Studies

To evaluate insights into the conformational changes of the compound **2c** with the H3 HA proteins 3EYM and 5T6N over time, MD simulations were performed via Desmond application implemented in Schrödinger Small Molecule Drug Discovery



Suite program (v.2022-1, Maestro, Schrödinger, Limited Liability Company, New York, 2022). The systems were firstly solvated by the predefined single point charge (SPC) water in the orthorhombic boundary condition at the distances of  $10 \times 10 \times 10$  Å, and the charges of the compound-protein complexes neutralized with adding  $\text{Na}^+/\text{Cl}^-$  ions with OPLS\_2005 force field on System Builder application. Then, the prepared complexes with 178721 and 164480 atoms for 3EYM and 5T6N structures (respectively) were applied to energy minimization using the steepest descent method with 310 K temperature and 1 atm pressure using Langevin as thermostat and barostat methods. MD simulations without any constraints were carried out for 50 ns with NPT ensemble class on MD application. For analyzing trajectories, comparing of the hydrogen bonding occupancy of the protein-ligand complexes and calculating the values of root mean square deviation (RMSD) and fluctuation (RMSF), the Simulation Interactions Diagram application were performed. The RMSD values between each snapshot with respect to the starting situation was plotted over during the 50 ns simulation.

## Author Contributions

**Gözde Çınar:** writing – original draft, investigation, conceptualization. **Zeynep Alikadoğlu:** investigation. **Özge Soylu-Eter:** writing – original draft, software. **Lieve Naesens:** investigation, writing – original draft, writing – review and editing. **Gökçe Cihan-Üstündağ:** writing – original draft, writing – review and editing, supervision.

## Acknowledgments

We would like to thank Professor Gültaze Çapan for sharing expertise in medicinal chemistry. L.N. wishes to thank the team of L. Persoons for dedicated technical assistance. This workstudy was supported by Scientific Research Projects Coordination Unit of Istanbul University (Grant Number: 32246).

## Conflicts of Interest

The authors declare no conflicts of interest.

## Data Availability Statement

The data that supports the findings of this study are available in the [Supporting Information](#) of this article.

## References

- Apaydın, Ç. B., M. Tansuyu, Z. Cesur, L. Naesens, and F. Göktas. 2021. "Design, Synthesis and Anti-Influenza Virus Activity of Furan-Substituted Spirothiazolidinones." *Bioorganic Chemistry* 112: 104958. <https://doi.org/10.1016/j.bioorg.2021.104958>.
- Baeyer, A. 1900. "Systematik Und Nomenclatur Bicyclischer Kohlenwasserstoffe." *Berichte Der Deutschen Chemischen Gesellschaft* 33, no. 3: 3771–3775. <https://doi.org/10.1002/cber.190003303187>.
- Batool, S., S. Chokkakula, and M. S. Song. 2023. "Influenza Treatment: Limitations of Antiviral Therapy and Advantages of Drug Combination Therapy." *Microorganisms* 11, no. 1: 183. <https://doi.org/10.3390/microorganisms11010183>.
- Blaising, J., S. J. Polyak, and E. I. Pécheur. 2014. "Arbidol as a Broad-Spectrum Antiviral: An Update." *Antiviral Research* 107, no. 1: 84–94. <https://doi.org/10.1016/j.antiviral.2014.04.006>.
- Bodian, D. L., R. B. Yamasaki, R. L. Buswell, J. F. Stearns, J. M. White, and I. D. Kuntz. 1993. "Inhibition of the Fusion-Inducing Conformational Change of Influenza Hemagglutinin by Benzoquinones and

Hydroquinones." *Biochemistry* 32, no. 2: 2967–2978. <https://doi.org/10.1021/bi00063a007>.

Chen, Z., Q. Cui, M. Caffrey, L. Rong, and R. Du. 2021. "Small Molecule Inhibitors of Influenza Virus Entry." *Pharmaceuticals* 14, no. 6: 587. <https://doi.org/10.3390/ph14060587>.

Cihan-Üstündağ, G., M. Zopun, E. Vanderlinden, et al. 2020. "Superior Inhibition of Influenza Virus Hemagglutinin-Mediated Fusion by Indole-Substituted Spirothiazolidinones." *Bioorganic & Medicinal Chemistry* 28, no. 1: 115130. <https://doi.org/10.1016/j.bmc.2019.115130>.

Cihan-Üstündağ, G., Ç. Acar, L. Naesens, G. Erköse-Genç, and D. Şatana. 2022. "Synthesis of New N-(3-oxo-1-thia-4-azaspiro[4.5]decan-4-yl)pyridine-3-carboxamide Derivatives and Evaluation of Their Anti-Influenza Virus and Antitubercular Activities." *Archiv der Pharmazie* 355, no. 10: e2200224. <https://doi.org/10.1002/ardp.202200224>.

Dong, G., C. Peng, J. Luo, et al. 2015. "Adamantane-Resistant Influenza A Viruses in the World (1902-2013): Frequency and Distribution of M2 Gene Mutations." *PLoS One* 10, no. 3: e0119115. <https://doi.org/10.1371/journal.pone.0119115>.

Van Dongen, M. J. P., R. U. Kadam, J. Juraszek, et al. 2019. "A Small-Molecule Fusion Inhibitor of Influenza Virus Is Orally Active in Mice." *Science* 363, no. 6431: eaar6221. <https://doi.org/10.1126/science.aar6221>.

Du, R., H. Cheng, Q. Cui, N. P. Peet, I. N. Gaisina, and L. Rong. 2021. "Identification of a Novel Inhibitor Targeting Influenza A Virus Group 2 Hemagglutinins." *Antiviral Research* 186: 105013. <https://doi.org/10.1016/j.antiviral.2021.105013>.

Göktaş, F., M. Özbil, N. Cesur, E. Vanderlinden, L. Naesens, and Z. Cesur. 2019. "Novel N-(1-thia-4-azaspiro[4.5]decan-4-yl) Carboxamide Derivatives as Potent and Selective Influenza Virus Fusion Inhibitors." *Archiv Der Pharmazie* 352, no. 11: e1900028. <https://doi.org/10.1002/ardp.201900028>.

Göktaş, F., E. Vanderlinden, L. Naesens, N. Cesur, and Z. Cesur. 2012. "Microwave Assisted Synthesis and Anti-Influenza Virus Activity of 1-Adamantyl Substituted N-(1-thia-4-azaspiro[4.5]decan-4-yl) Carboxamide Derivatives." *Bioorganic & Medicinal Chemistry* 20, no. 24: 7155–7159. <https://doi.org/10.1016/j.bmc.2012.09.064>.

Göktaş, F., E. Vanderlinden, L. Naesens, Z. Cesur, N. Cesur, and P. Taş. 2015. "Synthesis and Structure-Activity Relationship of N-(3-Oxo-1-Thia-4-Azaspiro[4.5]Decan-4-yl)Carboxamide Inhibitors of Influenza Virus Hemagglutinin Mediated Fusion." *Phosphorus, Sulfur and Silicon and the Related Elements* 190, no. 7: 1075–1087. <https://doi.org/10.1080/10426507.2014.965819>.

Harrington, W. N., C. M. Kackos, and R. J. Webby. 2021. "The Evolution and Future of Influenza Pandemic Preparedness." *Experimental & Molecular Medicine* 53, no. 5: 737–749. <https://doi.org/10.1038/s12276-021-00603-0>.

Hiesinger, K., D. Dar'In, E. Proschak, and M. Krasavin. 2021. "Spirocyclic Scaffolds in Medicinal Chemistry." *Journal of Medicinal Chemistry* 64, no. 1: 150–183. <https://doi.org/10.1021/acs.jmedchem.0c01473>.

Jiao, C., B. Wang, P. Chen, Y. Jiang, and J. Liu. 2023. "Analysis of the Conserved Protective Epitopes of Hemagglutinin on Influenza A Viruses." *Frontiers in Immunology* 14: 1086297. *Frontiers Media S.A.* <https://doi.org/10.3389/fimmu.2023.1086297>.

Jones, J. C., H. L. Yen, P. Adams, K. Armstrong, and E. A. Govorkova. 2023. "Influenza Antivirals and Their Role In Pandemic Preparedness." *Antiviral Research* 210: 105499. <https://doi.org/10.1016/j.antiviral.2022.105499>.

Kadam, R. U., and I. A. Wilson. 2017. "Structural Basis of Influenza Virus Fusion Inhibition by the Antiviral Drug Arbidol." *Proceedings of the National Academy of Sciences* 114, no. 2: 206–214. <https://doi.org/10.1073/pnas.1617020114>.

- Kang, Y., Y. Shi, and S. Xu. 2023. "Arbidol: The Current Demand, Strategies, and Antiviral Mechanisms." *Immunity, Inflammation and Disease* 11, no. 8: e984. <https://doi.org/10.1002/iid3.984>.
- Li, R., D. Song, Z. Zhu, H. Xu, and S. Liu. 2012. "An Induced Pocket for the Binding of Potent Fusion Inhibitor CL-385319 With H5N1 Influenza Virus Hemagglutinin." *PLoS One* 7, no. 8: e41956. <https://doi.org/10.1371/journal.pone.0041956>.
- Liu, S., R. Li, R. Zhang, et al. 2011. "CL-385319 Inhibits H5N1 Avian Influenza A Virus Infection By Blocking Viral Entry." *European Journal of Pharmacology* 660, no. 2–3: 460–467. <https://doi.org/10.1016/j.ejphar.2011.04.013>.
- Luo, G., R. Colonno, and M. Krystal. 1996. "Characterization of a Hemagglutinin-Specific Inhibitor of Influenza A Virus." *Virology* 226, no. 1: 66–76. <https://doi.org/10.1006/viro.1996.0628>.
- Luo, G., A. Torri, W. E. Harte, et al. 1997. "Molecular Mechanism Underlying the Action of a Novel Fusion Inhibitor of Influenza A Virus." *Journal of Virology* 71, no. 5: 4062–4070.
- Monto, A. S., and K. Fukuda. 2019. "Lessons From Influenza Pandemics of the Last 100 Years." *Clinical Infectious Diseases* 70, no. 5: 951–957. <https://doi.org/10.1093/cid/ciz803>.
- Müller, G., T. Berkenbosch, J. C. J. Benningshof, D. Stumpfe, and J. Bajorath. 2017. "Charting Biologically Relevant Spirocyclic Compound Space." *Chemistry – A European Journal* 23, no. 3: 703–710. <https://doi.org/10.1002/chem.201604714>.
- Neumann, G., and Y. Kawaoka. 2019. "Predicting the Next Influenza Pandemics." *Journal of Infectious Diseases* 219, no. 1: S14–S20. <https://doi.org/10.1093/infdis/jiz040/5304929>.
- Neumann, G., and Y. Kawaoka. 2024. "Highly Pathogenic H5N1 Avian Influenza Virus Outbreak In Cattle: the Knowns and Unknowns." *Nature Reviews Microbiology* 22, no. 9: 525–526. <https://doi.org/10.1038/s41579-024-01087-1>.
- Russell, R. J., P. S. Kerry, D. J. Stevens, et al. 2008. "Structure of Influenza Hemagglutinin In Complex With an Inhibitor of Membrane Fusion." *Proceedings of the National Academy of Sciences* 105, no. 46: 17736–17741. <https://doi.org/10.1073/pnas.0807142105>.
- Sempere Borau, M., and S. Stertz. 2021. "Entry of Influenza A Virus into Host Cells — Recent Progress and Remaining Challenges." *Current Opinion in Virology* 48: 23–29. Elsevier B.V. <https://doi.org/10.1016/j.coviro.2021.03.001>.
- Takashita, E., A. Meijer, A. Lackenby, et al. 2015. "Global Update on the Susceptibility of Human Influenza Viruses to Neuraminidase Inhibitors, 2013–2014." *Antiviral Research* 117: 27–38. <https://doi.org/10.1016/j.antiviral.2015.02.003>.
- Tang, G., X. Lin, Z. Qiu, et al. 2011. "Design and Synthesis of Benzenesulfonamide Derivatives As Potent Anti-Influenza Hemagglutinin Inhibitors." *ACS Medicinal Chemistry Letters* 2, no. 8: 603–607. <https://doi.org/10.1021/ml2000627>.
- Uyeki, T. M., D. S. Hui, M. Zambon, D. E. Wentworth, and A. S. Monto. 2022. "Influenza." *Lancet* 400, no. 10353: 693–706. [https://doi.org/10.1016/S0140-6736\(22\)00982-5](https://doi.org/10.1016/S0140-6736(22)00982-5).
- Vanderlinden, E., F. Göktas, Z. Cesur, et al. 2010. "Novel Inhibitors of Influenza Virus Fusion: Structure-Activity Relationship and Interaction With the Viral Hemagglutinin." *Journal of Virology* 84, no. 9: 4277–4288. <https://doi.org/10.1128/jvi.02325-09>.
- Varela, M. T., G. G. Dias, L. F. N. de Oliveira, et al. 2025. "Spirocyclic Compounds as Innovative Tools In Drug Discovery for Medicinal Chemists." *European Journal of Medicinal Chemistry* 287: 117368. <https://doi.org/10.1016/j.ejmech.2025.117368>.
- Vrijens, P., S. Noppen, T. Boogaerts, et al. 2019. "Influenza Virus Entry via the GM3 Ganglioside-Mediated Platelet-Derived Growth Factor Receptor  $\beta$  Signalling Pathway." *Journal of General Virology* 100, no. 4: 583–601. <https://doi.org/10.1099/jgv.0.001235>.
- Wright, Z. V. F., N. C. Wu, R. U. Kadam, I. A. Wilson, and D. W. Wolan. 2017. "Structure-Based Optimization and Synthesis of Antiviral Drug Arbidol Analogues With Significantly Improved Affinity to Influenza Hemagglutinin." *Bioorganic & Medicinal Chemistry Letters* 27, no. 16: 3744–3748. <https://doi.org/10.1016/j.bmcl.2017.06.074>.
- Wu, N. C., and I. A. Wilson. 2020. "Structural Biology of Influenza Hemagglutinin: An Amaranthine Adventure." *Viruses* 12, no. 9: 1053. <https://doi.org/10.3390/v12091053>.
- Zhao, X., R. Li, Y. Zhou, et al. 2018. "Discovery of Highly Potent Pinanamine-Based Inhibitors against Amantadine- and Oseltamivir-Resistant Influenza A Viruses." *Journal of Medicinal Chemistry* 61, no. 12: 5187–5198. <https://doi.org/10.1021/acs.jmedchem.8b00042>.
- Zheng, Y., C. M. Tice, and S. B. Singh. 2014. "The Use of Spirocyclic Scaffolds in Drug Discovery." *Bioorganic & Medicinal Chemistry Letters* 24, no. 16: 3673–3682. <https://doi.org/10.1016/j.bmcl.2014.06.081>.

## Supporting Information

Additional supporting information can be found online in the Supporting Information section.